INTERNATIONAL JOURNAL OF CLIMATOLOGY
Int. J. Climatol. **36**: 3191–3206 (2016)
Published online 18 November 2015 in Wiley Online Library
(wileyonlinelibrary.com) DOI: 10.1002/joc.4547

RMetS
Royal Meteorological Society

Diagnosing links between atmospheric moisture and extreme daily precipitation over the UK

Richard P. Allan,[a]* David A. Lavers[b] and Adrian J. Champion[a]
[a] *Department of Meteorology, University of Reading, UK*
[b] *Scripps Institution of Oceanography, University of California, San Diego, La Jolla, CA, USA*

ABSTRACT: Atmospheric moisture characteristics associated with the heaviest 1% of daily rainfall events affecting regions of the British Isles are analysed over the period 1997–2008. A blended satellite/rain-gauge data set (GPCP-1DD) and regionally averaged daily rain-gauge observations (HadUKP) are combined with the ERA Interim reanalysis. These are compared with simulations from the HadGEM2-A climate model which applied observed sea surface temperature and realistic radiative forcings. Median extreme daily rainfall across the identified events and locations is larger for GPCP (32 mm day^{-1}) than HadUKP and the simulations (~25 mm day^{-1}). The heaviest observed and simulated daily rainfall events are associated with increased specific humidity and horizontal transport of moisture (median 850 hPa specific humidity of ~6 g kg^{-1} and vapour transport of ~150 g kg^{-1} m s^{-1} for both observed and simulated events). Extreme daily rainfall events are less common during spring and summer across much of the British Isles, but in the south east region, they contribute up to 60% of the total number of distinct extreme daily rainfall events during these months. Compared to winter events, the summer events over south east Britain are associated with a greater magnitude and more southerly location of moisture maxima and less spatially extensive regions of enhanced moisture transport. This contrasting dependence of extreme daily rainfall on moisture characteristics implies a range of driving mechanisms that depend upon location and season. Higher spatial and temporal resolution data are required to explore these processes further, which is vital in assessing future projected changes in rainfall and associated flooding.

KEY WORDS hydrological cycle; Europe; water; precipitation; satellite; climate model

Received 22 April 2015; Revised 22 September 2015; Accepted 29 September 2015

1. Introduction

Flooding associated with heavy rainfall can lead to extensive damage to society (Penning-Rowsell, 2014), the severity of which is anticipated to increase as the climate warms in response to rising atmospheric concentrations of greenhouse gases (Pall *et al.*, 2011; Arnell and Gosling, 2014). The intensification of rainfall is primarily explained by increases in atmospheric moisture with warming (Trenberth *et al.*, 2003). Over middle latitude regions, atmospheric rivers (ARs), narrow bands of strong moisture transport within the warm sector of extra-tropical cyclones (Browning and Pardoe, 1973; Zhu and Newell, 1998; Dacre *et al.*, 2014; Gimeno *et al.*, 2014), have been linked with heavy rainfall and high river flows in the winter half year (Ralph *et al.*, 2006; Dettinger *et al.*, 2011; Lavers *et al.*, 2011; Neiman *et al.*, 2013). The strength of these synoptic features is anticipated to grow as temperatures rise due to concurrent increases in atmospheric moisture (Dettinger *et al.*, 2011; Lavers *et al.*, 2013; Warner *et al.*, 2015).

In the United Kingdom, in addition to flooding that is linked to large-scale synoptic features, intense sub-daily rainfall also plays an important role in flooding, particularly during the summer season. For example, a stationary convergence line of intense convection over Cornwall influenced flooding in Boscastle on the 16 August 2004 (Golding *et al.*, 2005) while complex frontal structure within a polar low led to devastating flooding in Lynmouth during the 15 August 1952 (McGinnigle, 2002). Thunderstorms in warm, moist southerly flows or 'Spanish plumes' (Carlson and Ludlam, 1968) also commonly lead to intense summer thunderstorms.

While ARs are not found to contribute substantially to heavy rainfall during the summer half of the year (Champion *et al.*, 2015), the intensification of summer rainfall extremes is expected to increase with a warming of climate (Kendon *et al.*, 2014) through contrasting mechanisms operating at finer time and space scales than during the winter (Lenderink and van Meijgaard, 2010; Berg *et al.*, 2013). While it is important to analyse and understand the full intensity/duration characteristics of rainfall (Kendon *et al.*, 2014; Blenkinsop *et al.*, 2015), here we concentrate on characterizing moisture and its transport by the winds associated with heavy daily rainfall totals across the British Isles region.

The aim of this study is to analyse the heaviest 1% of daily rainfall events from a blended satellite/gauge data set and regionally averaged daily rain-gauge observations,

* Correspondence to: R. P. Allan, Department of Meteorology, University of Reading, Earley Gate, PO Box 243, Reading, Berkshire, RG6 6BB, UK. E-mail: r.p.allan@reading.ac.uk

sampling grid points across the British Isles, and to assess the associated moisture characteristics, diagnosed from atmospheric reanalyses. In particular, are there threshold values for specific humidity and moisture transport associated with the most extreme rainfall events and how do these vary by geographical region and season? Simulations from an atmospheric climate model applying observed sea surface temperature fields and realistic radiative forcings are compared and evaluated over the period 1997–2008. The data sets and methodology are outlined in the following section.

2. Methods and data

2.1. GPCP precipitation data

Daily gridded precipitation from the Global Precipitation Climatology Project (GPCP; Huffman *et al.*, 2009) 1 Degree Daily (1DD) data set (Huffman *et al.*, 2001) version 1.2 is considered over the British Isles and surrounding region (10°W–2°E, 50°–58°N) for the period October 1996 to present. This combines infra-red satellite data with an atmospheric model to generate daily rainfall which are subsequently scaled such that monthly totals are equal to the 2.5×2.5 degree latitude and longitude monthly estimates from the Satellite-Gauge GPCP monthly product version 2.2 (Huffman *et al.*, 2001, 2009); the monthly mean daily precipitation is scaled to match monthly averaged rain-gauge measurements over land and satellite infra-red/microwave retrievals over the ocean.

Because the processing of satellite retrievals will inevitably introduce biases and errors into the estimates of rainfall, an alternative approach would be to consider daily rain-gauge measurements. However, in this exploratory analysis, we decided to exploit the satellite-based estimates because these provide spatially and temporally consistent coverage across the wider British Isles region at spatial scales consistent with climate models.

2.2. HadUKP precipitation data

The Met Office Hadley Centre and Climatic Research Unit regionally averaged daily rain-gauge data set (HadUKP) is provided over nine UK regions as described by Alexander and Jones (2000). These data are quality controlled by ensuring homogeneity of observations within each region and applying a two-stage averaging procedure to account for changing gauge network characteristics. The data set covers the period 1931–present, but we focus on the recent period 1997–2008 to enable consistent comparison with the other data sets considered. It is cautioned by Alexander and Jones (2000) that regions containing variable station altitudes, such as north Scotland, are subject to higher uncertainty.

2.3. ERA Interim reanalysis data

The European Centre for Medium-range Weather Forecasts (ECMWF) Interim reanalysis (ERA Interim) is a state of the art reanalysis system covering the period 1979–present. An atmospheric weather forecast model with a fixed configuration is physically constrained by observations using four-dimensional data assimilation. Vertical profiles of temperature and water vapour from satellite and conventional observations are used by the assimilation system, and the resulting analysis provides comprehensive diagnostics of atmospheric and surface properties every 6-h at various forecast lead times. A detailed description of ERA Interim is provided elsewhere (Dee *et al.*, 2011).

While some variables are strongly constrained by assimilated variables, such as water vapour and temperature, others such as cloud and precipitation are dependent upon the realism of the model parametrizations. We considered 0.75×0.75 degree latitude/longitude resolution 6-h data, extracting specific humidity (q), zonal wind (u) and meridional wind (v) components at 850 hPa and also column-integrated water vapour (IWV, units of $\mathrm{kg\,m^{-2}}$ which approximates to mm assuming a water density of $1000\ \mathrm{kg\,m^{-3}}$) and westerly and southerly vertically integrated horizontal water vapour transport (IVT) computed by Berrisford *et al.* (2011). These variables were diagnosed at the model analysis time (every 6-h) ensuring that the water vapour profiles and transports are strongly dependent upon the assimilation of water vapour variables and are therefore physically realistic.

2.4. HadGEM-2 atmospheric model simulation

The atmospheric component of the Hadley Centre Global Environment Model version 2 (HadGEM2-A; Collins *et al.* (2011)) is considered, using ensemble member 1 of the Atmospheric Model Inter-comparison Project (AMIP) experiment, part of the fifth phase of the Coupled Model Inter-comparison Project [CMIP5; Taylor *et al.* (2011)]. The simulation prescribes observationally based sea surface temperature and sea ice fields and realistic radiative forcings over the period 1979–2008. Considering additional models and ensemble members would provide more details on the role of unforced variability and model specification in precipitation and moisture variability. However, in this exploratory analysis, a single experiment is deemed sufficient to highlight the primary characteristics of moisture and its links to precipitation in a state of the art simulation. The simulation is conducted at a resolution of 1.25° latitude by 1.88° longitude and 6-h q, u, v and pressure (p) fields on 38 model-levels and daily mean sea level pressure fields (MSLP) were obtained. Aspects of the water cycle and its response to climate change and the associated uncertainties are discussed in detail by Martin (2014).

2.5. Methodology

Employing 6-h diagnostics from HadGEM2-A and ERA Interim, vapour transport (V_T in units of $\mathrm{kg\,kg^{-1}}$ times $\mathrm{m\,s^{-1}}$) at 850 hPa was approximated as a moisture-weighted wind (6-h 850 hPa q from HadGEM2-A was vertically interpolated using

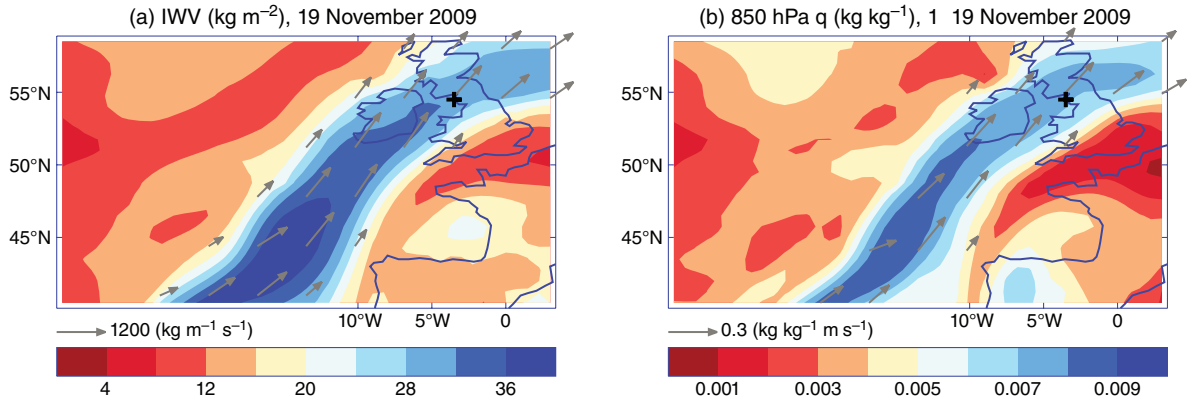

Figure 1. ERA Interim moisture and moisture transport fields associated with the heaviest daily rainfall event in the GPCP-1DD record (1996–2013) over the Cumbrian region (denoted by +): (a) column-integrated water vapour (IWV, kg m^{-2}, colours) and integrated water vapour transport (arrows show direction and length denotes magnitude, shown only for values greater than 400 kg m^{-1} s^{-1}), (b) 850 hPa specific humidity (q in kg kg^{-1}, colours) and vapour transport (arrows, plotted for $V_T > 0.1$ (kg kg^{-1})(m s^{-1})).

model-level data):

$$V_T = \sqrt{(qu)^2 + (qv)^2} \quad (1)$$

This diagnostic is physically linked with the column-IVT which is computed as:

$$\mathrm{IVT} = \sqrt{\left(\frac{1}{g}\int_{p_s}^{0} qu\,\mathrm{d}p\right)^2 + \left(\frac{1}{g}\int_{p_s}^{0} qv\,\mathrm{d}p\right)^2} \quad (2)$$

where p_s is the surface pressure and g is the acceleration due to gravity. Because IWV is dominated by the higher moisture amounts at low altitudes, the V_T diagnostic is considered a good proxy for IVT (see Section 3) and comparable diagnostics have been previously linked to rainfall extremes (Lavers and Villarini, 2014).

Moisture fields for the wider north Atlantic region (30°W–4°E, 40°–60°N) were extracted for days experiencing the heaviest rainfall (the upper 1% of all daily rainfall totals including days without rainfall) at each grid box (the 43 wettest days over the 1997–2008 period) over the British Isles region (10°W–2°E, 50°–58°N). While daily-scale precipitation events can potentially be spread across 2 days, and may therefore not be identified as an extreme daily rainfall event, this is not considered likely to affect the conclusions of this study. Analysis of precipitation and moisture diagnostics was performed on the separate model and reanalysis grids to avoid further smoothing of fields through interpolation. This was considered acceptable because the precise location of the rainfall event is not required in assessing precipitation distributions; the associated regional moisture characteristics and spatial resolutions are broadly comparable.

Eight 6-h moisture fields coinciding with the extreme daily rainfall at each grid box on the coincident and preceding day were selected. From these eight fields, the one containing the largest moisture transport within ±1° in longitude and latitude of the grid box centre was retained. The surrounding grid boxes were considered to account for the convergence of moisture from the surrounding regions (e.g. Trenberth *et al.*, 2003; Dacre *et al.*, 2014); using a larger (±2°) spatial window did not noticeably alter the results. The following sections outline the analysis of moisture and moisture transport fields associated with heavy daily rainfall events over the British Isles and its dependence upon region and time of year.

3. Moisture characteristics associated with heavy daily rainfall

IWV is commonly used in identifying strong moisture transport episodes (e.g. Zhu and Newell, 1998; Lavers *et al.*, 2013) and has previously been linked with rainfall and flooding events (Zhu and Newell, 1998; Dettinger *et al.*, 2011; Lavers *et al.*, 2011; Lavers and Villarini, 2014). Lavers and Villarini (2014) found that combinations of IWV and wind diagnostics at the 850 hPa vertical level were reasonable proxies for IVT [see also Neiman *et al.* (2009) and Section 2.3]. The close association between IVT and V_T was first confirmed visually for a variety of events using the ERA Interim and GPCP data. To illustrate this, Figure 1 displays the moisture and moisture transport fields associated with the heaviest daily rainfall event in the GPCP-1DD record for the Cumbria (England) grid point (denoted by a +). This event (19 November 2009) has previously been identified as extreme in terms of the quantity of rainfall, the degree of resulting flooding and associated impacts (Lavers *et al.*, 2011).

Figure 1(a) shows a narrow (~200 km wide) band of high IWV (>32 kg m^{-2} to the south west of Cumbria) and associated region of strong IVT (~1200 kg m^{-1} s^{-1}) represented by arrows. This event has previously been identified by Lavers *et al.* (2011) as an example of an AR, associated with moisture convergence within the warm sector of its parent extra-tropical cyclone (Dacre *et al.*, 2014). This feature is also clearly visible in the 850 hPa specific humidity and V_T fields (Figure 1(b); V_T ~300 g kg^{-1} m s^{-1}) illustrating the utility of these simple diagnostics in identifying such features. Based upon these

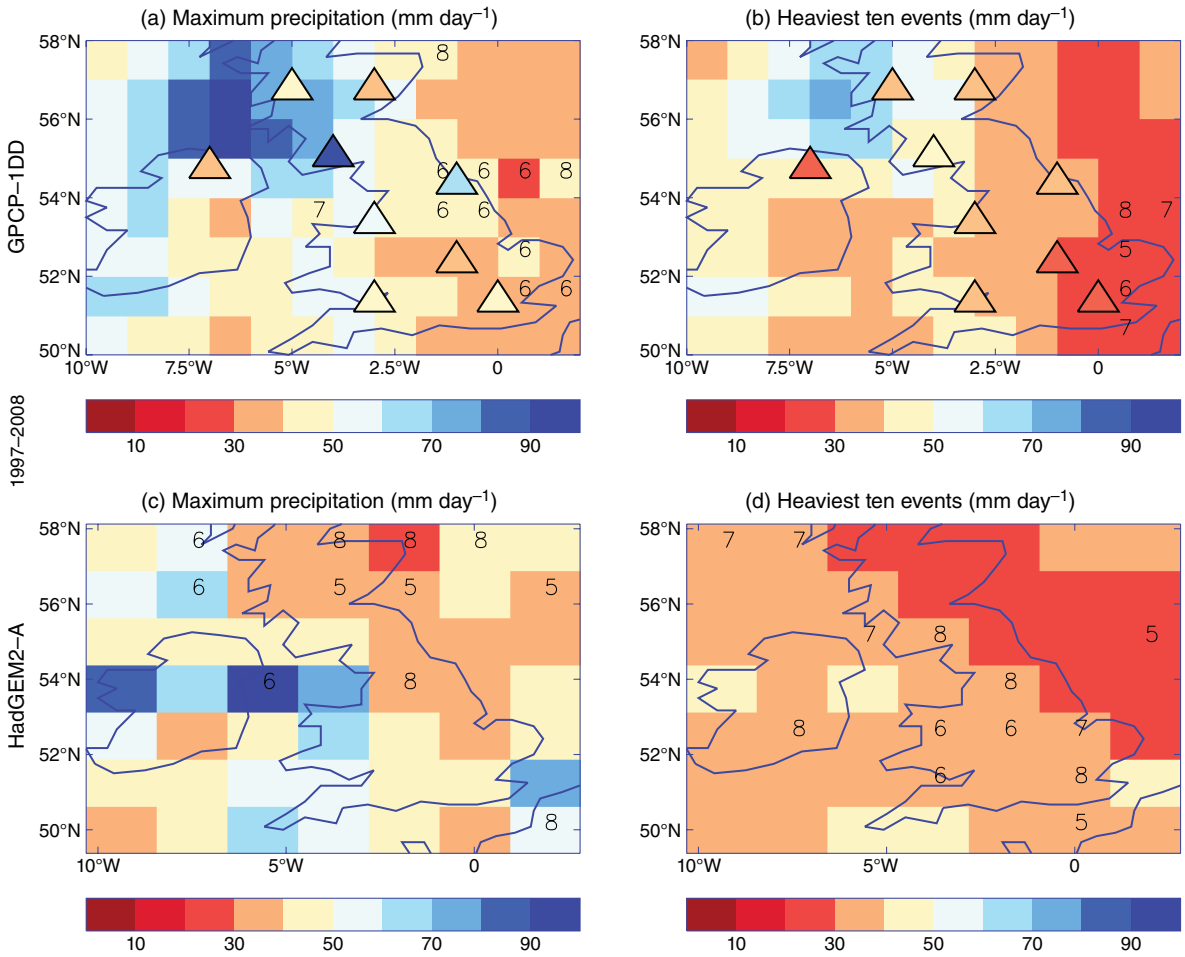

Figure 2. Maximum daily rainfall totals (a, c) and average rainfall for the heaviest ten daily events (both in mm day^{-1}) over the period 1997–2008 for HadUKP (triangles) and GPCP-1DD (a, b) and HadGEM2-A (c, d). Numbers denote the month in which the heaviest rainfall event occurs (a, c) or the most frequent month for the heaviest ten daily rainfall events (b, d) for GPCP and HadGEM2 and are plotted only for the extended summer period, May–August.

considerations and previous analysis (Lavers and Villarini, 2014), specific humidity and vapour transport at 850 hPa are used to investigate moisture characteristics associated with heavy daily rainfall events throughout the remainder of this study.

3.1. Maximum daily rainfall events

The maximum and average of the heaviest ten daily rainfall events during the period 1997–2008 are displayed in Figure 2 for the GPCP-1DD and HadGEM2-A simulation at each grid box over the British Isles region. The highest totals observed are found off the west coast of Scotland, reaching more than 90 mm day^{-1} and the lowest values in south east England (<40 mm day^{-1}). HadUKP observations are also displayed (triangles); while these observations and the HadGEM2-A simulations display a similar range in precipitation maxima, the distribution of values from south east to north west are less coherent than GPCP. For HadGEM2, the highest totals are found to the west of the British Isles, particularly around 54°N, while the lowest maxima are found in eastern Scotland (Figure 2(c)).

Also displayed in Figure 2 are grid points in which the maxima occurs during the extended summer months (May–August, represented by month numbers 5–8). This is also displayed for the ten heaviest daily rainfall events where the most frequently occurring month is displayed if it falls within the May–August period. It is evident from Figure 2(a) and (b) that the observed heaviest rainfall events tend to occur in the summer months preferentially across parts of eastern England. This is not apparent in the HadGEM2-A simulations and may result from the relatively low resolution of the simulations compared to the spatial scales of summer rainfall events; the realism of short duration rainfall is much improved in simulations of higher spatial resolution (Kendon *et al.*, 2014). The seasonality of maximum daily rainfall and the influence of moisture characteristics will be revisited in Section 3.4.

The number of extreme daily rainfall events per year are found to generally decline in number over the GPCP-1DD period (1997–2013) with notable high numbers of daily extreme rainfall events in 2000 over all grid boxes considered, in 2002 for central and southern grid boxes, 2004 for central and northern grid points and 2007 and 2012 in

Table 1. Median values of precipitation (P), specific humidity (q) and vapour transport (V_T) for the heaviest 1% of events over grid points representing six regions (as illustrated by □ symbols in Figures 3–8) and the average of all grid boxes in the British Isles region.

	GPCP	ERAI		HadGEM2-A		
Region (approximate longitude/latitude)	P (mm day^{-1})	$q \pm 1$ SD (g kg^{-1})	$V_T \pm 1$ SD (kg kg^{-1})(m s^{-1})	P (mm day^{-1})	$q \pm 1$ SD (g kg^{-1})	$V_T \pm 1$ SD (kg kg^{-1})(m s^{-1})
N Ireland (7°W, 54°N)	32.4	5.9 ± 1.3	0.16 ± 0.05	23.6	6.8 ± 1.4	0.17 ± 0.06
SW Scotland (4°W, 55°N)	36.2	5.8 ± 1.3	0.17 ± 0.05	23.8	6.9 ± 1.4	0.12 ± 0.06
Wales (4°W, 52°N)	30.4	6.3 ± 1.5	0.15 ± 0.06	23.9	7.3 ± 1.3	0.15 ± 0.06
E England (0°E, 53°N)	22.9	6.3 ± 1.6	0.13 ± 0.05	17.6	6.1 ± 1.6	0.11 ± 0.05
SW England (5°W, 50°N)	28.5	6.8 ± 1.3	0.16 ± 0.06	26.9	6.7 ± 1.2	0.15 ± 0.07
SE England (0°E, 51°N)	20.1	6.1 ± 1.6	0.12 ± 0.05	22.7	6.5 ± 1.3	0.11 ± 0.06
British Isles	32.0	6.0 ± 1.3	0.15 ± 0.05	24.9	6.4 ± 1.6	0.13 ± 0.06

Table 2. Median values of HadUKP precipitation (P) and ERA Interim specific humidity (q) and vapour transport (V_T) for the heaviest 1% of daily events over grid points representing nine regions and the unweighted average of all regions.

Region (and approximate longitude/latitude)	P (mm day^{-1})	$q \pm 1$ SD (g kg^{-1})	$V_T \pm 1$ SD (kg kg^{-1}) (m s^{-1})
Northern Scotland (NSP: 5°W, 57°N)	27.5	6.4 ± 1.3	0.14 ± 0.06
Eastern Scotland (ESP: 3°W, 57°N)	22.2	5.7 ± 1.7	0.11 ± 0.06
Northern Ireland (NIP: 7°W, 55°N)	21.3	5.8 ± 1.6	0.13 ± 0.05
Southern Scotland (SSP: 4°W, 55°N)	31.2	5.9 ± 1.5	0.15 ± 0.05
North West England (NWEP: 4°W, 55°N)	23.1	7.1 ± 1.4	0.15 ± 0.05
North East England (NEEP: 1°W, 54°N)	24.5	6.5 ± 1.8	0.11 ± 0.06
South West England (SWEP: 3°W, 51°N)	23.5	6.7 ± 1.3	0.16 ± 0.06
Central England (CEP: 1°W, 52°N)	19.4	6.6 ± 1.4	0.14 ± 0.05
South East England (SEEP: 0°E, 51°N)	20.8	6.5 ± 1.5	0.13 ± 0.06
Average	25.4	6.3 ± 1.5	0.14 ± 0.05

the eastern and south east England grid boxes (not shown). A persistent upper level trough during June/July 2007 and substantial evaporative fluxes over the Bay of Biscay led to a small number of intense precipitation events (Blackburn *et al.*, 2008; Allan and Zveryaev, 2011). In contrast, the autumn of 2000 and winter of 2000/2001 contributed heavy and sustained multi-day rainfall events affecting much of the United Kingdom, associated with a displacement in the North Atlantic jet stream (Pall *et al.*, 2011). The simulations do not capture year to year variability in the number of identified daily precipitation events; Pall *et al.* (2011) required a large number of ensemble members to build up robust statistics of rainfall and flooding associated with observed sea surface temperature patterns during Autumn 2000, indicating that unforced atmospheric variability contributes substantially to the number of extreme daily rainfall events.

3.2. Moisture characteristics associated with maximum daily rainfall

The characteristics of atmospheric moisture fields associated with heavy daily rainfall are analysed, focusing upon six representative grid boxes covering regions of the United Kingdom listed in Table 1. The choice of the grid boxes influence the characteristics of the heaviest events somewhat, but the composite fields and overall conclusions are not affected by the choice. Considering a longer time period of GPCP-1DD data (1997–2013) also does not influence the results significantly; precipitation and moisture amount and transport are within 5% of the values presented in Table 1.

The ERA Interim 850 hPa specific humidity fields and regions of strong V_T associated with the maximum observed GPCP daily rainfall events (1997–2008) are displayed for the six representative grid points (□ symbol) in Figure 3. A characteristic AR-like pattern is identified for the northern and western grid points (Figure 3(a)–(c)) with linear filaments of high specific humidity and coincident bands of strong vapour transport (denoted by arrows) broadly following the lines of MSLP isobars. As discussed by Dacre *et al.* (2014), ARs are associated with the cold front within the extra-tropical cyclone and are primarily formed through a convergence of local moisture rather than transport along the entire length of the filament. The substantial and sustained supply of moisture combined with uplift over mountains can generate extreme multi-day rainfall and associated winter flooding (e.g. Lavers *et al.*, 2011; Neiman *et al.*, 2013). The intensity of the rainfall is explained by the seeder–feeder mechanism (Bader and Roach, 1977) in which precipitating upper level cloud, formed through the cyclone's dynamical processes (Browning and Pardoe, 1973), falls through moisture-laden orographic stratus, fuelled by the massive quantities of moisture transported by the wind within the AR region. A similar but less linear AR-like structure is also present for the heaviest daily rainfall event affecting the south west England grid point (Figure 3(e)).

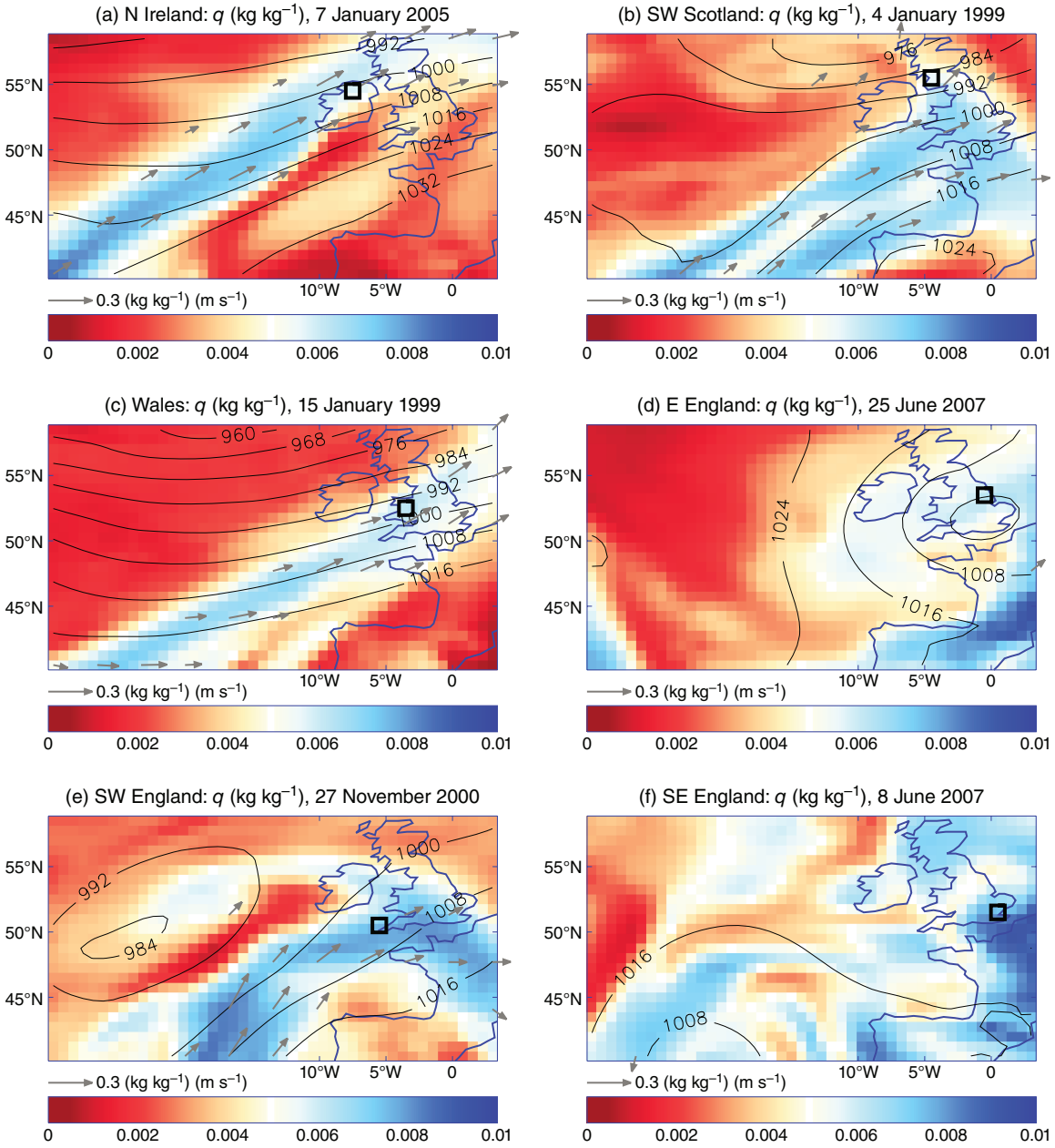

Figure 3. ERA Interim 850 hPa specific humidity (kg kg^{-1}, colours) and water vapour transport [arrows, plotted for $V_T > 0.1$ (kg kg^{-1})(m s^{-1})] associated with the heaviest daily rainfall event in the GPCP-1DD record over the period 1997–2008 (date plotted) over regions denoted by □: (a) Northern Ireland, (b) Southern Scotland, (c) Wales, (d) Eastern England, (e) South West England and (f) South East England. Contours of daily pressure fields at mean sea level are over-plotted.

The western and northern extremes discussed above occurred during winter months (late November–January). However, the heaviest observed rainfall events for the east and south east England grid boxes (Figure 3(d) and (f)) were recorded in June and the ERA Interim moisture fields do not exhibit the AR-like pattern characteristic of the northern and western regions. Champion *et al.* (2015) find that less than 20% of the extreme daily summer rainfall events are linked with ARs. While moisture content is generally high (>6 g kg^{-1} at 850 hPa) for the south and east grid boxes, isobars are spaced further apart compared to the northern/western events, implying weaker winds; consequently, moisture transport at the 100 km scale is not strong. There is also indication of cyclonic flows over or to the south east of these grid boxes with an associated easterly flow transporting moisture in from the North Sea, as opposed to the south-westerly flow influencing the northern and western regions. In the case of the 8 June 2007 (Figure 3(f)), a trough developed in an easterly air flow introducing thunderstorms to the south east of the United Kingdom. On the 25 June 2007 (Figure 3(d)), a developing area of low pressure became slow-moving over southern Britain, introducing a moist, easterly air flow from the North Sea and torrential rainfall over eastern regions of central and northern Britain.

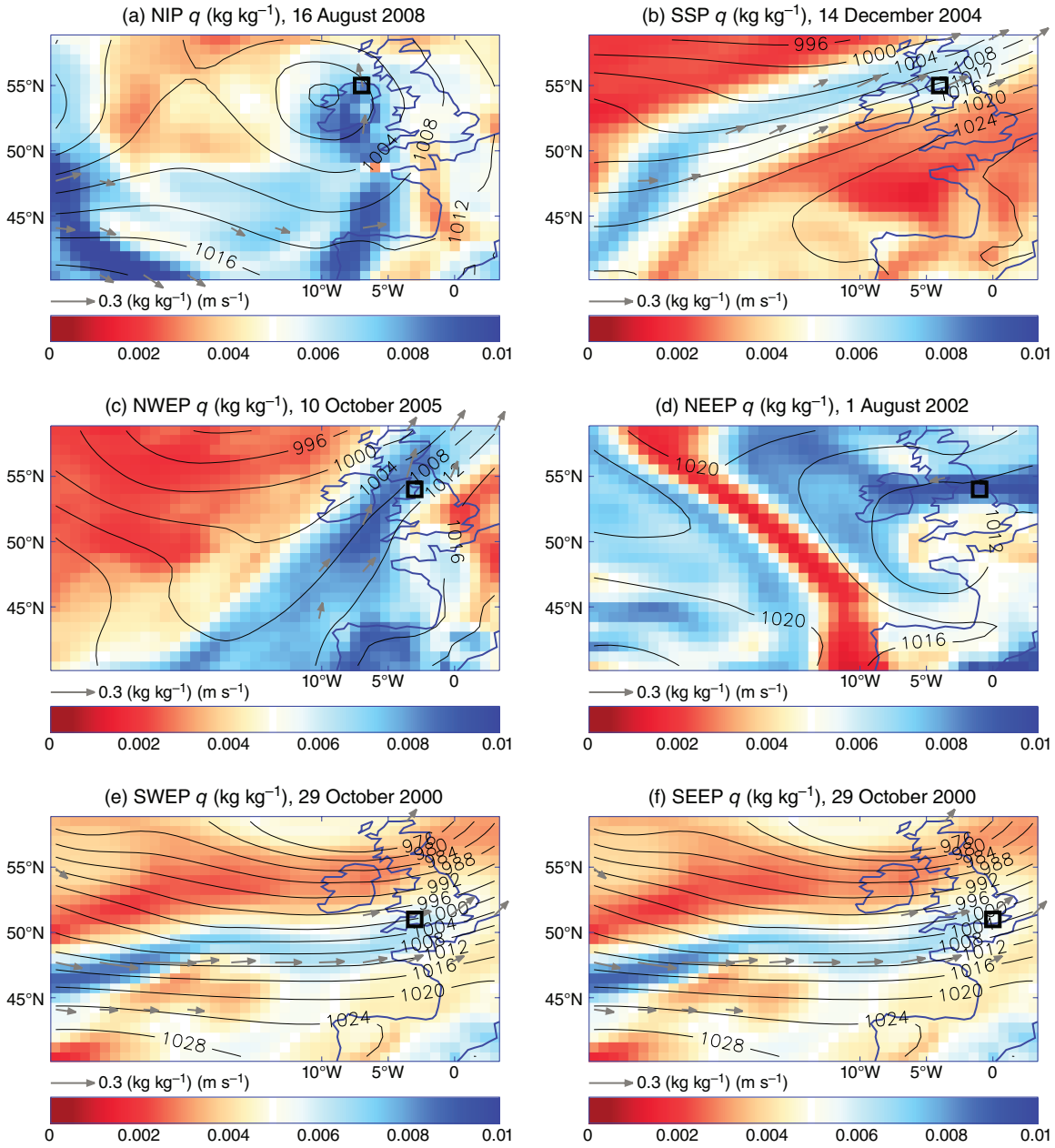

Figure 4. ERA Interim 850 hPa specific humidity (kg kg^{-1}, colours) and water vapour transport [arrows, plotted for $V_T > 0.1$ (kg kg^{-1})(m s^{-1})] associated with the heaviest daily rainfall event in the HadUKP record over the period 1997–2008 (date plotted) over HadUKP regions: (a) Northern Ireland (NIP), (b) Southern Scotland (SSP), (c) North West England (NWEP), (d) North East England (NEEP), (e) South West England (SWEP) and (f) South East England (SSEP).

The dates of the heaviest daily rainfall events identified in the HadUKP data set (Figure 4) do not coincide with the GPCP data (59% of the heaviest 1% of distinct daily rainfall events identified across all HadUKP regions are also identified as extreme events in the GPCP record). However, similar AR-like structures in the moisture fields are apparent in Figure 4 for the Southern Scotland region (14 December 2004), North West England (10 October 2005) and for the South West and South East regions (both 29 October 2000). The heaviest daily rainfall events occurred in summer months for Northern Ireland (16 August 2008; Figure 4(a)) associated with a developing cyclone that stalled to the west of the British Isles and the North East England region [1 August 2002; Figure 4(d)] associated with complex areas of low pressure to the south and east of the United Kingdom which introduced a strong easterly air flow bringing high moisture amounts from the North Sea.

The corresponding HadGEM2-A simulations of moisture characteristics associated with extreme daily rainfall are displayed in Figure 5. As previously discussed, standard spatial resolution models are capable of generating AR-like features (Allan *et al.*, 2014) although they may overestimate their frequency at lower spatial resolutions (Hagos *et al.*, 2015). These features are identified to coincide with the extreme daily rainfall

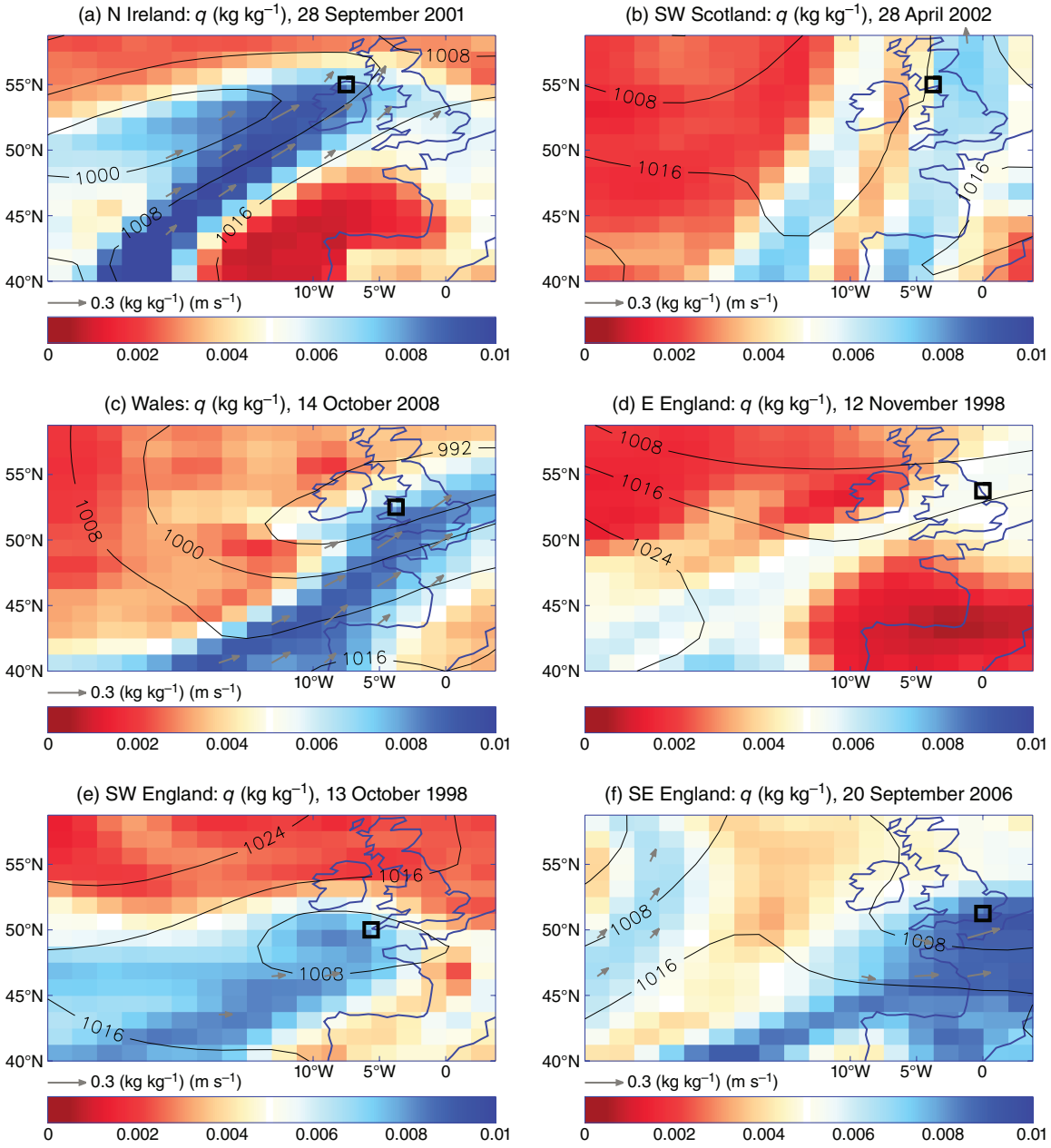

Figure 5. 850 hPa specific humidity (kg kg^{-1}, colours) and water vapour transport [arrows, plotted for $V_T > 0.1$ (kg kg^{-1})(m s^{-1})] associated with the heaviest daily rainfall event over the period 1997–2008 (date plotted) for HadGEM2-A for grid points denoted by □.

events affecting the western grid boxes in the HadGEM2-A simulations (Figure 5(a) and (c)). However, the simulated extreme events predominantly occur in Autumn (September–November), and there is generally less spatial coherence of the moisture characteristics compared to the observations.

Moisture characteristics associated with extreme daily rainfall indicate a role for ARs in both the observations and simulations considered. While an observed dependence on region and season is implied, the analysis is primarily illustrative in diagnosing such links between extreme daily rainfall on atmospheric precursors. The following sections consider composites of moisture characteristics associated with the heaviest 1% of daily events to seek more robust relationships between rainfall and atmospheric moisture patterns and the dependence on season.

3.3. Composites of moisture characteristics

Moisture characteristics are now assessed for the range of synoptic situations associated with the heaviest 1% of rainfall events from the observations (Figures 6 and 7) and HadGEM2-A (Figure 8). For each event, anomalies of 850 hPa specific humidity, V_T and daily mean MSLP are constructed by removing the pentad mean climatology (1997–2008) centred on the event date. Composites are formed by averaging over all events for each location. The composite mean values of specific humidity anomalies ($\overline{q'}$)

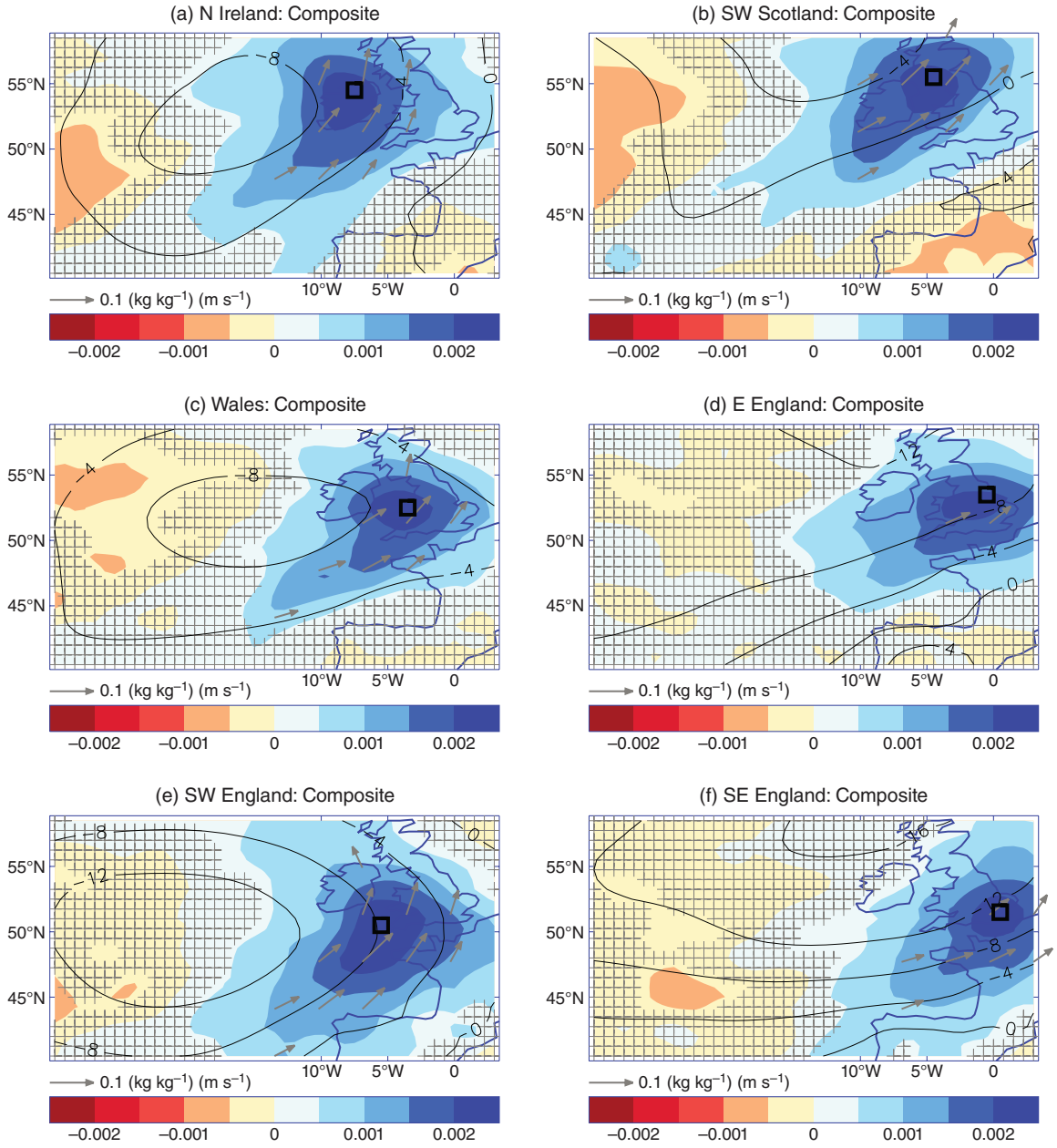

Figure 6. Composite of ERA Interim 850 hPa specific humidity anomaly (kg kg^{-1}, colours), water vapour transport anomaly [arrows, plotted for $\Delta V_T > 0.05$ (kg kg^{-1})(m s^{-1})] and contours of daily mean sea level pressure anomalies associated with the heaviest 1% of daily rainfall events in the GPCP-1DD record over the period 1997–2008 over regions denoted by □: (a) Northern Ireland, (b) Southern Scotland, (c) Wales, (d) Eastern England, (e) South West England and (f) South East England. Anomalies are calculated with respect to pentad climatology (1997–2008) centred on the each event. Hashing denotes where the specific humidity anomaly is not significantly different from zero (see text for details).

are deemed to be significantly different from zero at the 90% confidence level based upon a two-tailed t-test (e.g. Lavers *et al.*, 2015), assuming $n-1$ degrees of freedom, where $n = 43$:

$$|\overline{q'}| > A\sigma_{q'}/\sqrt{n} \quad (3)$$

where $\sigma_{q'}$ is the standard deviation of specific humidity anomalies across all events and $A = 1.68$ for 42 degrees of freedom. Hashing in Figures 6–8 denote where moisture anomalies are not significantly different from zero when applying this test. Considering a longer time period (1997–2013) for the GPCP data set does not alter the moisture maps substantially.

Both observations and simulations display positive moisture anomalies centred on the grid point considered and extending to the south west, with an associated region of strong vapour transport denoted by arrows. For the south and east regions for HadUKP (Figure 7d and f), this enhanced moisture transport appears less extensive in longitude. This implies (as expected) that different weather patterns are responsible for determining extreme rainfall in different locations and the seasonal dependence, which may also play a role, is considered later. Locations where specific humidity anomalies are not significant (denoted by hashing) generally do not coincide with the regions

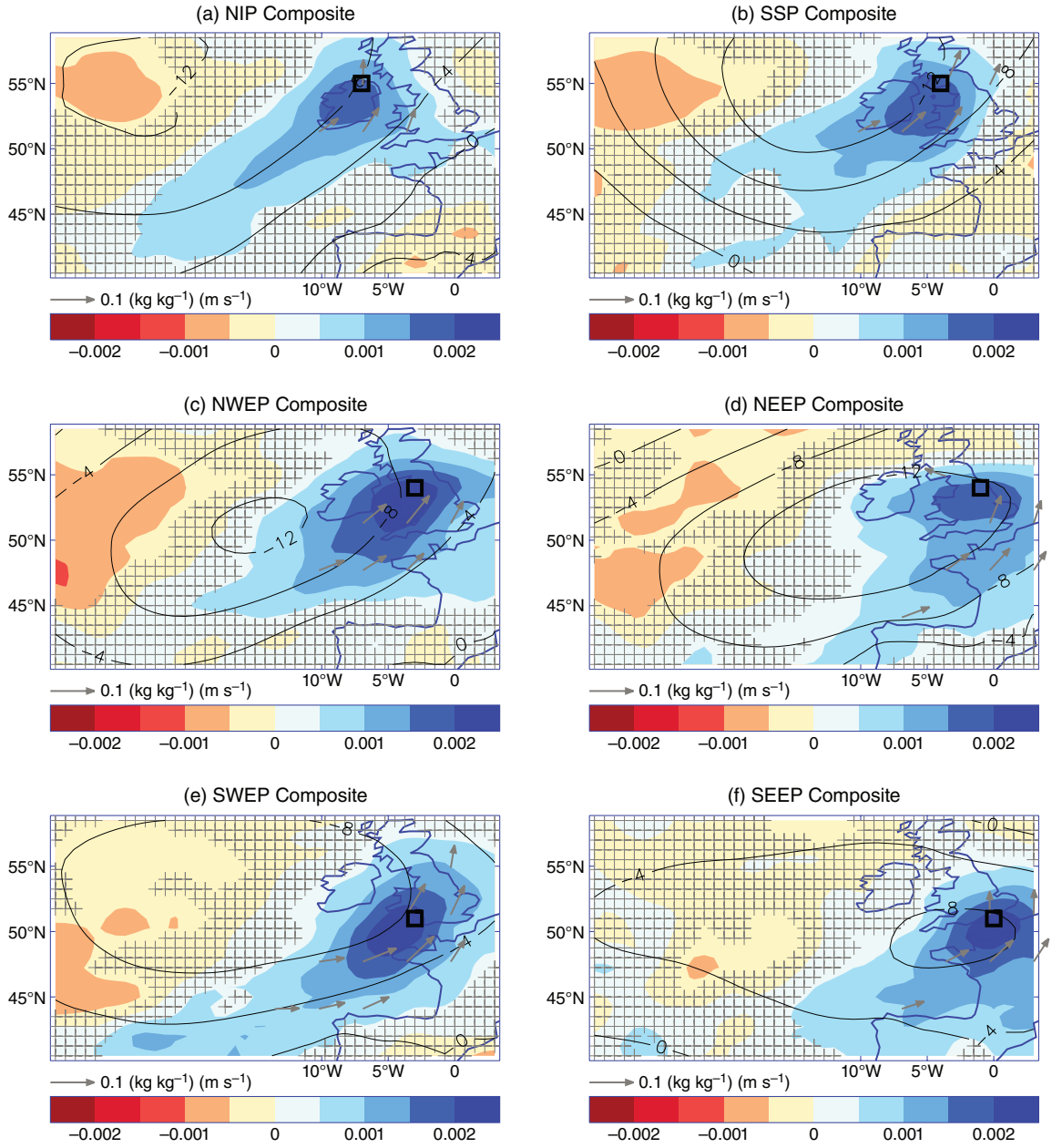

Figure 7. Composite of ERA Interim 850 hPa specific humidity anomaly ($kg\,kg^{-1}$, colours), water vapour transport anomaly [arrows, plotted for $\Delta V_T > 0.05$ $(kg\,kg^{-1})(m\,s^{-1})$] and contours of daily mean sea level pressure anomalies associated with the heaviest 1% of daily rainfall events in the HadUKP record over the period 1997–2008 over HadUKP regions: (a) Northern Ireland (NIP), (b) Southern Scotland (SSP), (c) North West England (NWEP), (d) North East England (NEEP), (e) South West England (SWEP) and (f) South East England (SSEP).

of strong moisture transport and high specific humidity. Anomalous low pressure is associated with the heaviest rainfall events. For the observations, the negative MSLP anomaly is positioned to the west of the western locations considered (Figure 6(a), (c), and (e)) while for eastern locations (Figure 8(b), (d), and (f)) and the simulations (Figure 8) the pressure anomaly tends to be to the north west of the locations considered.

Comparing Figures 6–8, the area covered by specific humidity anomalies greater than 0.002 $kg\,kg^{-1}$ appears larger in HadGEM2-A compared to ERA Interim. This is also evident in the mean specific humidity composites, which have higher values in HadGEM2-A (not shown) although this is not apparent for the grid point median values shown in Table 1. Centred on the grid boxes considered, the largest differences (of about 1 $g\,kg^{-1}$) are apparent over the more northern grid boxes although median values of specific humidity are within 1 standard deviation at all locations considered in Table 1. Moisture transport is comparable between HadGEM2-A and the observations [ranging from 0.11 $(kg\,kg^{-1})(m\,s^{-1})$ in eastern grid boxes up to 0.17 $(kg\,kg^{-1})(m\,s^{-1})$ for western grid boxes with similar values when conditioning on HadUKP extreme daily rainfall] as shown by comparing median values of V_T between regions (Tables 1 and 2). This can be explained by stronger winds depicted by the reanalysis

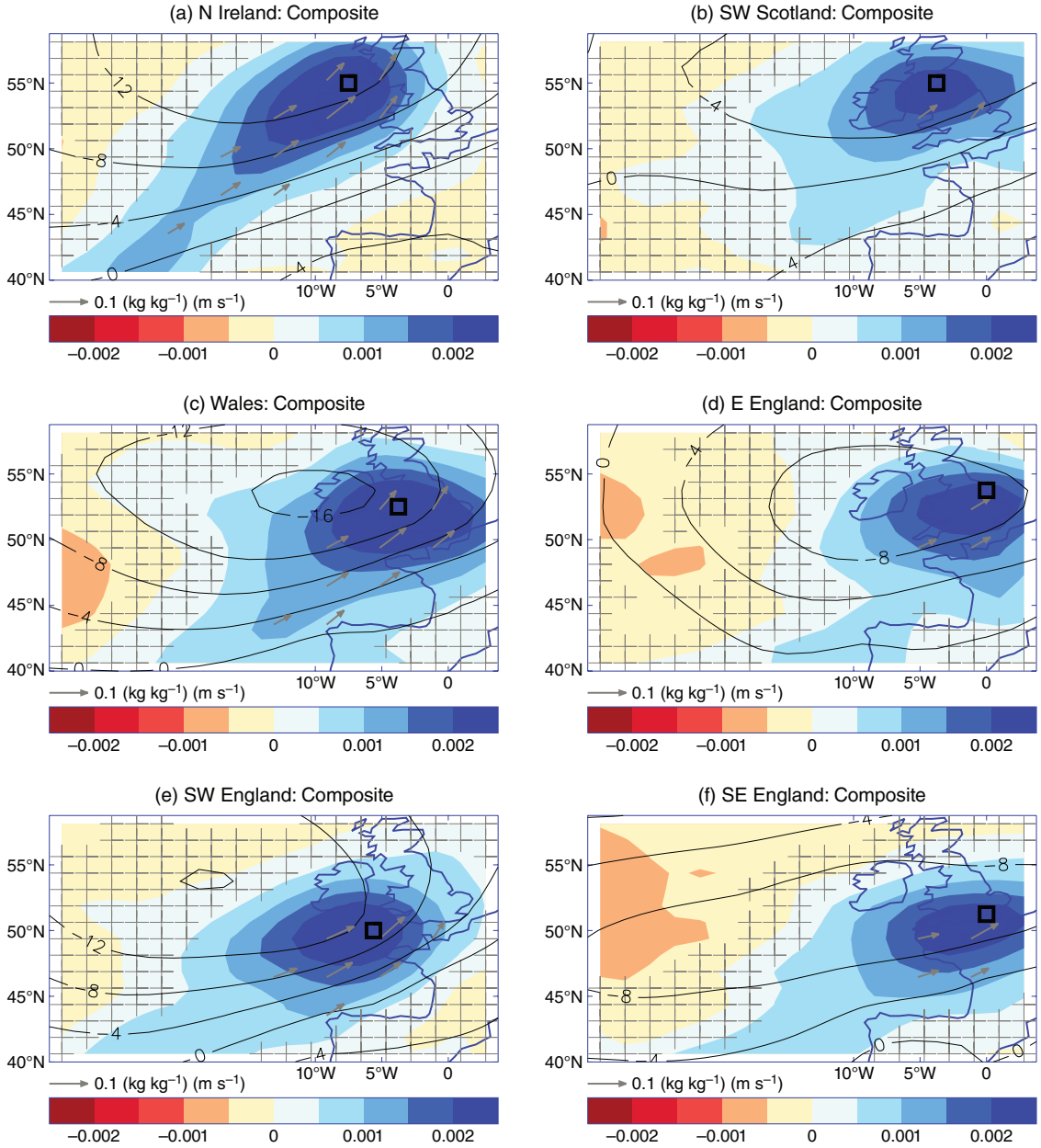

Figure 8. Composite of 850 hPa specific humidity anomaly (kg kg^{-1}, colours), water vapour transport anomaly [arrows, plotted for $\Delta V_T > 0.05$ (kg kg^{-1})(m s^{-1})] and contours of daily mean sea level pressure anomalies associated with the heaviest 1% of daily rainfall events over the period 1997–2008 for HadGEM2-A for grid points denoted by □.

related to the closer spacing of isobars in ERA Interim (not shown). HadUKP and simulated median precipitation are generally lower than indicated by GPCP observations by around 20% on average (Tables 1 and 2) apart from for south east England as also indicated in Figure 2. HadUKP depicts a median precipitation over the heaviest 1% events of 25.4 mm day^{-1} across all nine UK regions (Table 2), comparable to HadGEM2 for the wider British Isles region (Table 1).

3.4. Dependence of rainfall events on season

Analysis of moisture fields associated with the heaviest observed daily rainfall events from GPCP (Figure 3) is suggestive of contrasting spatial structure and seasonal characteristics between grid boxes representing south east and eastern England and the western and northern regions. The dependence of these fields on season is now investigated further.

Normalized distributions of the 1% of heaviest precipitation events by month are displayed in Figure 9. This was computed where daily events covering multiple grid boxes count either as a single event ('distinct') or as multiple events ('non-distinct'). Using the longer GPCP record (1997–2013) altered the magnitude of normalized frequency by no more than 0.04. For both methods, the highest frequency of heavy rainfall events occurs in December for the GPCP observations and simulations. Comparing Figure 9(a) and (b), the proportion of all

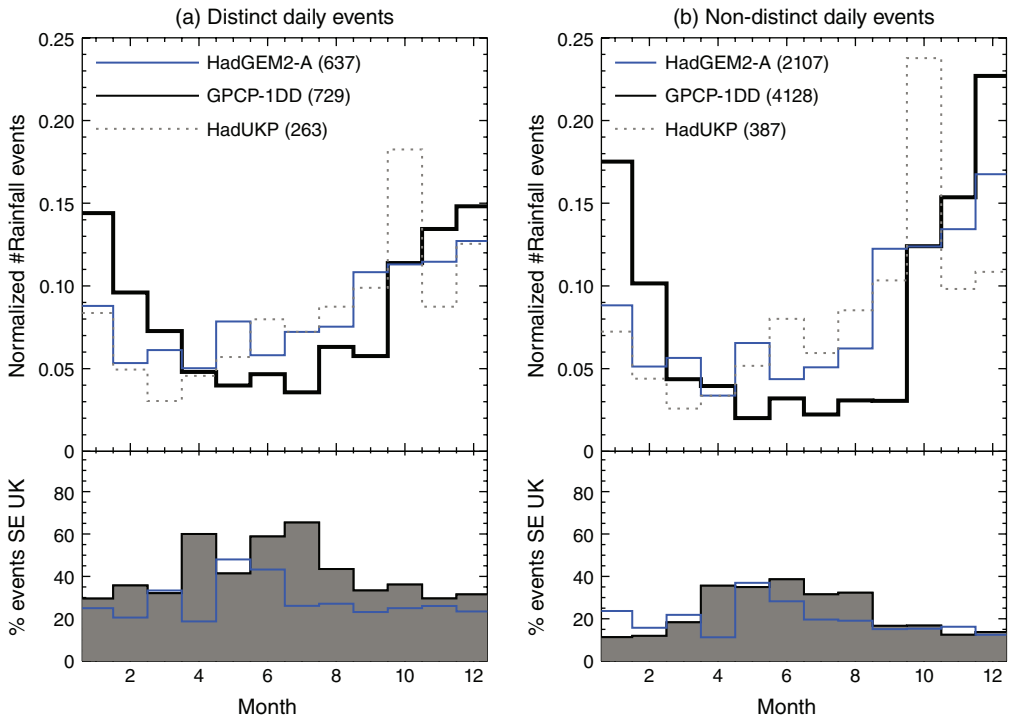

Figure 9. Histogram depicting the normalized distribution by month of the heaviest 1% of rainfall from all grid boxes covering the British Isles (top panels) and the percentage of events in each month being contributed by the south east region (2°W–2°E, 50°–54°N) for GPCP observations (black or grey shading) and HadGEM2-A simulations (blue). Data from the nine HadUKP regions are also shown in the upper panels (dashed). Histograms are shown for (a) distinct events (removing duplicate events which affect multiple grid boxes) and (b) all events (including duplicates). Numbers within the panels denote the total number of events considered; in (b) this equals 1% of the number of days multiplied by the number of grid boxes.

events falling in December drops substantially when considering only distinct events (falling from about 23% of all events to 15% of all distinct events in the observations). This indicates that December events tend to affect more grid boxes simultaneously (influencing a wider spatial area) compared with other months. Interestingly, the HadUKP observations show October as the month with the highest frequency of events that also affect multiple regions; this is primarily determined by northern and western regions. The fewest observed events occur in the summer half of the year (April–September) although this minimum period is shifted around 1–2 months earlier in the HadGEM2-A simulations and the HadUKP observations which display fewer November–March events and more May–September/October events compared to GPCP-1DD. Further work is required to understand how the scale dependence of extreme rainfall events across seasons combined with the varying spatial resolutions of the data sets contributes to this discrepancy.

The contribution of the south east region (2°W–2°E, 50°–54°N, around 17–18% of the of the number of grid boxes contained in the British Isles region) to the overall number of observed heaviest daily precipitation events is shown in the lower panels of Figure 9 for GPCP and HadGEM2. This contribution is largest in the April–August period, explaining over 40% of all distinct events in each month, although these months contain relatively few extreme rainfall events compared to the winter half of the year. The increased contribution of the south east region to the total number of extreme rainfall events across the British Isles in summer is less clear for HadGEM2-A (Figure 9, lower panels) although the south east region contributes the most to the total number of monthly events in May (over 50% of the distinct events). For the HadUKP data set, the south east region does not contribute to a greater extent in spring/summer to UK-wide rainfall events (not shown).

The larger contribution of the south east region to total number of GPCP observed distinct events (Figure 9(a)) compared to non-distinct events (Figure 9(b)) each month suggests that events in the south east are less spatially extensive and coherent. This may also reflect the position of the south east region relative to the prevailing winds and the rest of the British Isles region, yet a similar increase in proportional contribution is not evident in the HadGEM2-A data.

Based upon the results of Figures 3 and 9, the grid box representing the south east England region is further analysed with respect to the seasonality of moisture characteristics associated with heavy rainfall events. Figure 10 shows composites of specific humidity, V_T and MSLP associated with the heaviest 1% of precipitation events for the south east England grid box for each season. In contrast to Figures 6–8, absolute values rather than anomalies are considered to highlight differences between seasons. The number of daily events contributing to each composite are labelled in the panel titles.

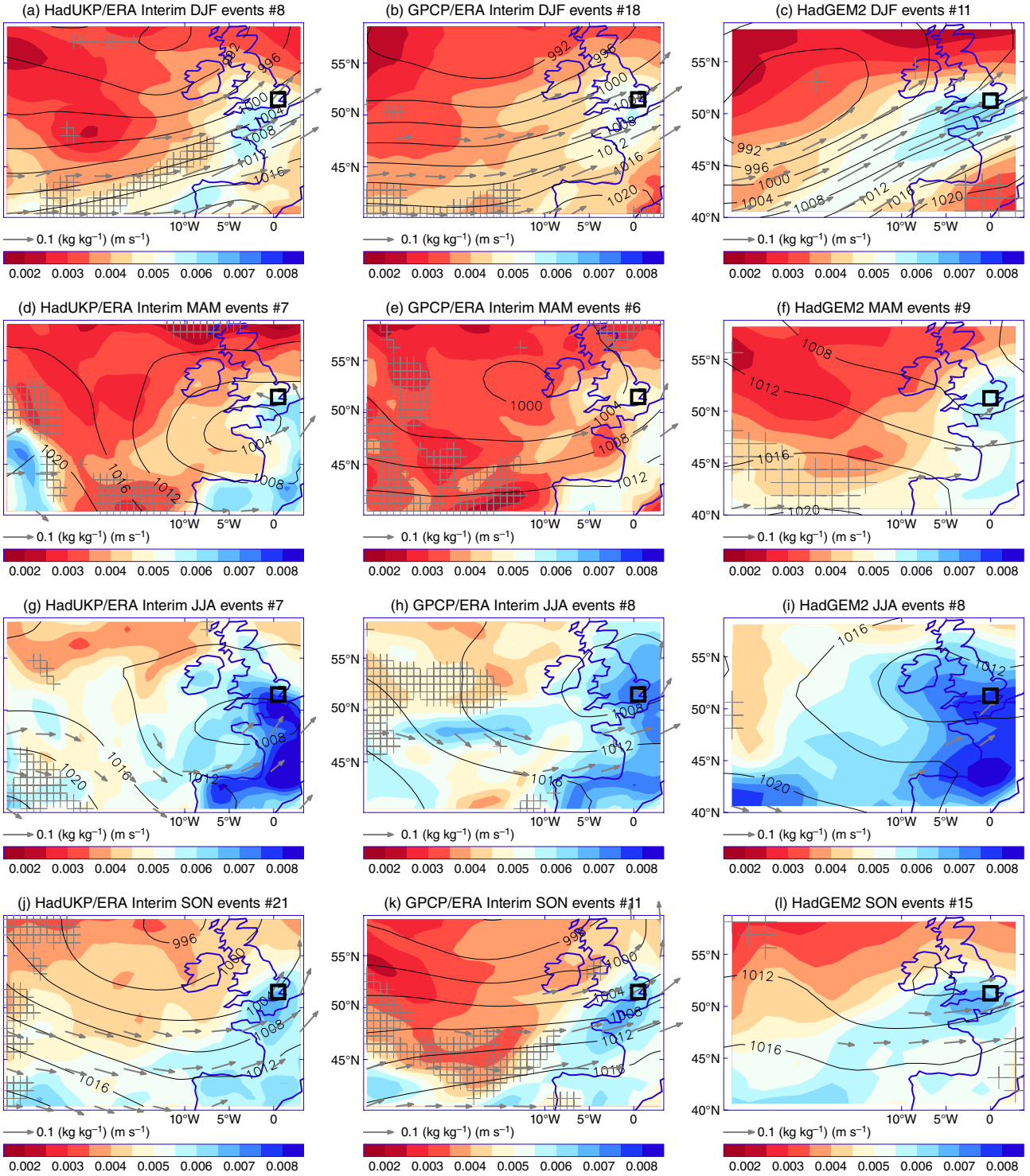

Figure 10. Composite of HadUKP/ERA Interim (a, d, g, j), GPCP-1DD/ERA Interim (b, e, h, k) and HadGEM2-A (c, f, i, l) 850 hPa specific humidity, q (kg kg^{-1}, colours), water vapour transport [arrows, plotted for $V_T > 0.06$ (kg kg^{-1})(m s^{-1})] and daily mean sea-level pressure fields associated with the heaviest 1% of daily rainfall events over the south east England grid point (□) 1997–2008 for December–February (a–c), March–May (d–f), June–August (g–i) and September–November (j–l). Hashing denotes where the standard deviation of q is more than half its mean.

Extensive regions of enhanced V_T are evident during winter (DJF) and associated with strong winds implied by the tightly packed isobars of MSLP (Figure 10(a) and (b)). While ERA Interim depicts a more westerly flow and northerly pressure minimum, the overall structure is comparable to the model simulation. A broadly similar spatial structure is present in autumn (SON) in ERA Interim (Figure 10(j) and (k)). While moisture characteristics are similar in SON, the region of strong V_T is less extensive in the HadGEM2-A simulations and the pressure gradient weaker implying weaker wind fields (Figure 10(l)). Furthermore, the model simulates seven

fewer DJF events and 4 more SON events than GPCP, qualitatively consistent with the analysis of the British Isles region as a whole (Figure 9).

Specific humidity is particularly high in summer, explained by the potential for higher water vapour content due to higher saturation vapour pressure associated with the warmer conditions in summer (e.g. Zveryaev *et al.*, 2008) combined with high relative humidity associated with the synoptic conditions leading up to the heavy rainfall events. The spatial distribution of moisture in summer (JJA) differs to the other seasons. Compared to winter, pressure gradients are slacker and the spatial structure more data set dependent in spring/summer. Also there are greater quantities of moisture evident over a band extending from the Iberian peninsula, through France and into south east England. Combined with cyclonic conditions over the southern United Kingdom, this implies a transport of moisture more from the south than the west as experienced in other seasons. Vapour transport is generally weak, however, indicating that heavy rainfall may be more reliant on local sources of moisture compared to winter and autumn. This is apparent in the synoptic situation associated with the heaviest observed daily rainfall event shown in Figure 3(f) and was a feature of summer 2007 (e.g. Blackburn *et al.*, 2008; Pearson *et al.*, 2015). It is planned in future work to evaluate the precursor conditions to summer extreme rainfall and flooding events in more detail through analysis of additional thermodynamic variables including convective available potential energy (e.g. Lepore *et al.*, 2015).

Where contrasting synoptic features contribute to the composites, there are likely to be weaker and less spatially coherent distributions of specific humidity and surface pressure patterns. This may be particularly applicable to the relatively few summer events (eight in both GPCP and simulations) compared with autumn or winter (more than ten events per season). Nevertheless, the region in which the standard deviation of specific humidity across composite members is greater than 50% of the mean (denoted by hashed regions in Figure 10) are relatively small, in particular for HadGEM2-A, and are located away from the higher humidity regions; this indicates that moisture characteristics associated with extreme daily rainfall are reasonably robust.

4. Conclusions

The heaviest 1% of daily rainfall in multiple grid points covering the British Isles are analysed in a blended satellite/rain-gauge dataset (GPCP-1DD), regionally averaged daily rain-gauge observations (HadUKP) and a climate model simulation applying prescribed observed sea surface temperature and realistic radiative forcing (HadGEM2-A) over the period 1997–2008. The primary aims were to (1) diagnose characteristics of moisture and its transport associated with heavy daily rainfall, (2) assess the dependence upon region and season and (3) to evaluate the realism of these characteristics simulated by a climate model.

Precipitation from the heaviest daily events range from around 30–40 mm day^{-1} in eastern parts of the United Kingdom up to around 90 mm day^{-1} for western Scotland in the observations and over eastern Ireland in the simulations (relating to a June event in this case). Considering all of the 1% most extreme daily rainfall events across the United Kingdom, median values of specific humidity at 850 hPa are ∼6–7 g kg^{-1} while vapour transport at the same pressure level ranges between ∼0.1–0.2 (kg kg^{-1})(m s^{-1}).

Many of the heaviest observed daily rainfall events over the United Kingdom are associated with narrow bands of increased low-altitude moisture content and transport, commonly termed ARs, which form in the warm sector of extra-tropical cyclones (Ralph *et al.*, 2006; Dettinger *et al.*, 2011; Lavers *et al.*, 2011; Dacre *et al.*, 2014; Gimeno *et al.*, 2014). This association is qualitatively represented by HadGEM2-A simulations as demonstrated through analysis of the most extreme events and through compositing. However, the simulations tend to exhibit a wider region of increased moisture amounts centred on the grid point experiencing heavy daily rainfall. Because the model underestimates the number of winter events, which occur under colder conditions, this may contribute to the higher average moisture.

Fewer extreme daily precipitation events occur during the summer half year (April–September) than the winter half year for the GPCP observations. This is consistent with evidence from river flow records over the United Kingdom (Lavers *et al.*, 2011) although catchment size and characteristics also play a role because small-scale intense events are unlikely to influence river flow in large slow-responding catchments. HadUKP observations and HadGEM2 simulations also reproduce the fewer number of summer events although the period of minimum activity occurs around 1–2 months earlier in the year and the number of events occurring in January and February is fewer than in the GPCP data set. The proportion of all observed events falling in December (GPCP) or October (HadUKP) drops substantially when removing duplicate events affecting multiple regions, indicating that October and December events are associated with larger storm systems that than during other months depending on data set.

The south east UK region contributes to a greater extent towards the total number of GPCP observed monthly events during spring/summer, around 60% in April, June and July. This is less apparent in the other data sets although this region contributes more than half of the distinct daily precipitation events affecting the British Isles region in May for HadGEM2. It is important to note that the scale dependence of events is represented quite differently by all data sets: the GPCP data are strongly influenced by infra-red and microwave satellite retrievals while HadUKP uses a large area average of point measurements (rain-gauges).

The spring/summer extreme daily rainfall events in the south east UK region are found to be associated with slacker pressure gradients and weaker wind and moisture

transport fields than the autumn/winter seasons. Cyclonic southerly flow during the summer season can often be associated with intense thunderstorms (e.g. Carlson and Ludlam, 1968; Lewis and Gray, 2010). Moisture amounts are greater in summer due to the higher saturated vapour pressure, associated with the warmer conditions, combined with high relative humidity; the region of enhanced atmospheric moisture extends further to the south as opposed to the more south-westerly orientation applying in the autumn/winter. The lack of extensive regions of enhanced moisture transport during the spring/summer may reflect a more local source of moisture for supplying intense rainfall, for example as part of intense convective events.

The established strong link between atmospheric moisture and rainfall intensity (Trenberth *et al.*, 2003; O'Gorman and Schneider, 2009; Lenderink and van Meijgaard, 2010) means that heavy rainfall events will intensify in a warmer climate because water vapour is strongly constrained by thermodynamics to increase with warming. Lavers *et al.* (2013) demonstrated an increase in the intensity of moisture transport over the United Kingdom with warming, explained by simulated increases in moisture at around 7% per °C of warming, a rate anticipated from the Clausius Clapeyron equation when applied to surface conditions and assuming that relative humidity does not change substantially. This is expected to apply in particular to the winter half year where there is a close connection between strong moisture transport associated with large-scale synoptic features, rainfall intensity and peak river flows which lead to a heightened risk of flooding (Dettinger *et al.*, 2011; Lavers *et al.*, 2011; Lavers and Villarini, 2014). The applicability to summer rainfall is less clear because smaller spatial scale thunderstorms and embedded convection, which depend upon atmospheric stability in addition to moisture availability and transport, are important in determining extreme rainfall (e.g. Berg *et al.*, 2013). It is only by using high spatial resolution simulations that the relevant processes may be realistically captured (Kendon *et al.*, 2014; Blenkinsop *et al.*, 2015).

It is plausible that enhanced latent heating from additional condensation of water droplets in a warmer climate may further invigorate individual storms leading to rainfall increases greater than anticipated from the Clausius Clapeyron scaling of about 7% K^{-1} applicable near to the surface (Lenderink and van Meijgaard, 2008; Berg *et al.*, 2013). However, at larger scales, the extra atmospheric heating stabilizes temperature lapse rates, inhibiting increases in precipitation. Therefore, future changes in rainfall are liable to be strongly dependent upon the precise intensity/duration characteristics, and it is therefore imperative to further investigate this using high spatial and temporal resolution data. Extending the present analysis to consider hourly rainfall intensities using surface rain-rate data and additional diagnostics relating to available potential energy is required to elucidate the controls on summer rainfall.

Acknowledgements

We thank two anonymous reviewers for taking the time to evaluate and provide comments on our manuscript which was substantially improved as a result. GPCP-1DD v1.2 data were extracted from ftp://rsd.gsfc.nasa.gov/pub/1dd-v1.2/, HadUKP observations were provided by the Met Office and Climatic Research Unit at the University of East Anglia, available at http://www.metoffice.gov.uk/hadobs/hadukp/, ERA Interim 6-h data were downloaded from http://apps.ecmwf.int/datasets/ and HadGEM2-A 6-h data were extracted from the British Atmospheric Data Centre (http://badc.nerc.ac.uk/home). This work was funded by the Natural Environment Research Council SINATRA project (NE/K00896X/1).

References

Alexander LV, Jones PD. 2000. Updated precipitation series for the U.K. and discussion of recent extremes. *Atmos. Sci. Lett.* **1**: 142–150, doi: 10.1006/asle.2000.0016.

Allan RP, Zveryaev II. 2011. Variability in the summer season hydrological cycle over the Atlantic-Europe region 1979-2007. *Int. J. Climatol.* **31**: 337–348, doi: 10.1002/joc.2070.

Allan R, Liu C, Zahn M, Lavers D, Koukouvagias E, Bodas-Salcedo A. 2014. Physically consistent responses of the global atmospheric hydrological cycle in models and observations. *Surv. Geophys.* **35**: 533–552, doi: 10.1007/s10712-012-9213-z.

Arnell NW, Gosling SN. 2014. The impacts of climate change on river flood risk at the global scale. *Clim. Change*, doi: 10.1007/s10584-014-1084-5.

Bader MJ, Roach WT. 1977. Orographic rainfall in warm sectors of depressions. *Q. J. R. Meteorol. Soc.* **103**: 269–280, doi: 10.1002/qj.49710343605.

Berg P, Moseley C, Haerter JO. 2013. Strong increase in convective precipitation in response to higher temperatures. *Nat. Geosci.* **6**: 181–185, doi: 10.1038/ngeo1731.

Berrisford P, Kållberg P, Kobayashi S, Dee D, Uppala S, Simmons AJ, Poli P, Sato H. 2011. Atmospheric conservation properties in era-interim. *Q. J. R. Meteorol. Soc.* **137**(659): 1381–1399, doi: 10.1002/qj.864.

Blackburn M, Methven J, Roberts N. 2008. Large-scale context for the UK floods in summer 2007. *Weather* **63**(9): 280–288.

Blenkinsop S, Chan SC, Kendon EJ, Roberts NM, Fowler HJ. 2015. Temperature influence on intense UK hourly precipitation and dependency on large-scale circulation. *Environ. Res. Lett.* **10**: 054021, doi: 10.1088/1748-9326/10/5/054021.

Browning KA, Pardoe CW. 1973. Structure of low-level jet streams ahead of mid-latitude cold fronts. *Q. J. R. Meteorol. Soc.* **99**(422): 619–638, doi: 10.1002/qj.49709942204.

Carlson TN, Ludlam FH. 1968. Conditions for the occurrence of severe local storms. *Tellus* **20**: 203–226, doi: 10.1111/j.2153-3490.1968.tb00364.x.

Champion AJ, Allan RP, Lavers DA. 2015. Atmospheric rivers don't explain uk summer extreme rainfall. *J. Geophys. Res.* **120**: 6731–6741, doi: 10.1002/2014JD022863.

Collins WJ, Bellouin N, Doutriaux-Boucher M, Gedney N, Halloran P, Hinton T, Hughes J, Jones CD, Joshi M, Liddicoat S, Martin G, O'Connor F, Rae J, Senior C, Sitch S, Totterdell I, Wiltshire A, Woodward S. 2011. Development and evaluation of an Earth-system model – HadGEM2. *Geosci. Model. Dev. Discuss.* **4**: 997–1062, doi: 10.5194/gmdd-4-997-2011.

Dacre HF, Clark PA, Martinez-Alvarado O, Stringer MA, Lavers DA. 2014. How do atmospheric rivers form? *Bull. Am. Meteorol. Soc.* **96**: 1243–1255, doi: 10.1175/bams-d-14-00031.1.

Dee DP, Uppala SM, Simmons AJ, Berrisford P, Poli P, Kobayashi S, Andrae U, Balmaseda MA, Balsamo G, Bauer P, Bechtold P, Beljaars ACM, van de Berg L, Bidlot J, Bormann N, Delsol C, Dragani R, Fuentes M, Geer AJ, Haimberger L, Healy SB, Hersbach H, Hólm EV, Isaksen L, Kållberg P, Köhler M, Matricardi M, McNally AP, Monge-Sanz BM, Morcrette J-J, Park B-K, Peubey C, de Rosnay P, Tavolato C, Thépaut J-N, Vitart F. 2011. The ERA-Interim

reanalysis: configuration and performance of the data assimilation system. *Q. J. R. Meteorol. Soc.* **137**: 553–597, doi: 10.1002/qj.828.
Dettinger MD, Ralph FM, Das T, Neiman PJ, Cayan DR. 2011. Atmospheric rivers, floods and the water resources of California. *Water* **3**: 445–478, doi: 10.3390/w3020445.
Gimeno L, Nieto R, Vazquez M, Lavers DA. 2014. Atmospheric rivers: a mini-review. *Front. Earth Sci.* **2**, doi: 10.3389/feart.2014.00002.
Golding B, Clark P, May B. 2005. The boscastle flood: meteorological analysis of the conditions leading to flooding on 16 August 2004. *Weather* **60**: 230–235, doi: 10.1256/wea.71.05.
Hagos S, Leung LR, Yang Q, Zhao C, Lu J. 2015. Resolution and dynamical core dependence of atmospheric river frequency in global model simulations. *J. Clim.* **28**: 2764–2776, doi: 10.1175/JCLI-D-14-00567.1.
Huffman GJ, Adler RF, Morrissey MM, Bolvin DT, Curtis S, Joyce R, McGavock B, Susskind J. 2001. Global precipitation at one-degree daily resolution from multisatellite observations. *J. Hydrometeorol.* **2**: 36–50.
Huffman GJ, Adler RF, Bolvin DT, Gu G. 2009. Improving the global precipitation record: GPCP version 2.1. *Geophys. Res. Lett.* **36**: L17808, doi: 10.1029/2009GL040000.
Kendon EJ, Roberts NM, Fowler HJ, Roberts MJ, Chan SC, Senior CA. 2014. Heavier summer downpours with climate change revealed by weather forecast resolution model. *Nat. Clim. Change* **4**: 570–576, doi: 10.1038/nclimate2258.
Lavers DA, Villarini G. 2014. The relationship between daily european precipitation and measures of atmospheric water vapour transport. *Int. J. Climatol.* **35**: 2187–2192, doi: 10.1002/joc.4119.
Lavers DA, Allan RP, Wood EF, Villarini G, Brayshaw DJ, Wade AJ. 2011. Winter floods in Britain are connected to atmospheric rivers. *Geophys. Res. Lett.* **38**: L23803, doi: 10.1029/2011GL049783.
Lavers DA, Allan RP, Villarini G, Lloyd-Hughes B, Brayshaw DJ, Wade AJ. 2013. Future changes in atmospheric rivers and their implications for winter flooding in Britain. *Environ. Res. Lett.* **8**: 034010.
Lavers DA, Hannah DM, Bradley C. 2015. Connecting large-scale atmospheric circulation, river flow and groundwater levels in a chalk catchment in Southern England. *J. Hydrol.* **523**: 179–189, doi: 10.1016/j.jhydrol.2015.01.060.
Lenderink G, van Meijgaard E. 2008. Increase in hourly precipitation extremes beyond expectations from temperature changes. *Nat. Geosci.* **1**: 511–514, doi: 10.1038/ngeo262.
Lenderink G, van Meijgaard E. 2010. Linking increases in hourly precipitation extremes to atmospheric temperature and moisture changes. *Environ. Res. Lett.* **5**: 025208, doi: 10.1088/1748-9326/5/2/025208.
Lepore C, Veneziano D, Molini A. 2015. Temperature and cape dependence of rainfall extremes in the eastern united states. *Geophys. Res. Lett.* **42**: 74–83, doi: 10.1002/2014gl062247.
Lewis MW, Gray SL. 2010. Categorisation of synoptic environments associated with mesoscale convective systems over the UK. *Atmos. Res.* **97**: 194–213, doi: 10.1016/j.atmosres.2010.04.001.
Martin G. 2014. Quantifying and reducing uncertainty in the large-scale responses of the water cycle. *Surv. Geophys.* **35**: 553–575, doi: 10.1007/s10712-012-9203-1.
McGinnigle JB. 2002. The 1952 Lynmouth floods revisited. *Weather* **57**: 235–242, doi: 10.1256/004316502760195894.
Neiman PJ, Gottas DJ, White AB, Gutman SI, Ralph FM. 2009. A water vapour flux tool for precipitation forecasting. *Proc. ICE – Water Manage.* **162**: 83–94, doi: 10.1680/wama.2009.162.2.83.
Neiman PJ, Ralph FM, Moore BJ, Hughes M, Mahoney KM, Cordeira JM, Dettinger MD. 2013. The landfall and inland penetration of a flood-producing atmospheric river in Arizona. Part I: observed synoptic-scale, orographic, and hydrometeorological characteristics. *J. Hydrometeorol.* **14**(2): 460–484, doi: 10.1175/jhm-d-12-0101.1.
O'Gorman PA, Schneider T. 2009. The physical basis for increases in precipitation extremes in simulations of 21st-century climate change. *Proc. Natl. Acad. Sci.* **106**: 14773–14777.
Pall P, Aina T, Stone DA, Stott PA, Nozawa T, Hilberts AGJ, Lohmann D, Allen MR. 2011. Anthropogenic greenhouse gas contribution to flood risk in England and Wales in autumn 2000. *Nature* **470**: 382–385, doi: 10.1038/nature09762.
Pearson KJ, Shaffrey LC, Methven J, Hodges KI. 2015. Can a climate model reproduce extreme regional precipitation events over England and Wales? *Q. J. R. Meteorol. Soc.* **141**: 1466–1472, doi: 10.1002/qj.2428.
Penning-Rowsell EC. 2014. A realistic assessment of fluvial and coastal flood risk in England and Wales. *Trans. Inst. Br. Geogr.* **40**: 44–61, doi: 10.1111/tran.12053.
Ralph FM, Neiman PJ, Wick GA, Gutman SI, Dettinger MD, Cayan DR, White AB. 2006. Flooding on California's Russian river: role of atmospheric rivers. *Geophys. Res. Lett.* **33**: L13801, doi: 10.1029/2006gl026689.
Taylor KE, Stouffer RJ, Meehl GA. 2011. An overview of CMIP5 and the experiment design. *Bull. Am. Meteorol. Soc.* **93**: 485–498, doi: 10.1175/BAMS-D-11-00094.1.
Trenberth KE, Dai A, Rasmussen RM, Parsons DB. 2003. The changing character of precipitation. *Bull. Am. Meteorol. Soc.* **84**: 1205–1217.
Warner MD, Mass CF, Salathé EP. 2015. Changes in winter atmospheric rivers along the North American west coast in CMIP5 climate models. *J. Hydrometeorol.* **16**: 118–128, doi: 10.1175/jhm-d-14-0080.1.
Zhu Y, Newell RE. 1998. A proposed algorithm for moisture fluxes from atmospheric rivers. *Mon. Weather Rev.* **126**: 725–735, doi: 10.1175/1520-0493(1998)126<0725:apafmf>2.0.co;2.
Zveryaev II, Wibig J, Allan RP. 2008. Contrasting interannual variability of atmospheric moisture over Europe during cold and warm seasons. *Tellus A* **60**(1): 32–41, doi: 10.1111/j.1600-0870.2007.00283.x.